Gadolinium-Functionalized Aggregation-Induced Emission Dots as Dual-Modality Probes for Cancer Metastasis Study

*Kai Li, Dan Ding, Chandrasekharan Prashant, Wei Qin, Chang-Tong Yang, Ben Zhong Tang, and Bin Liu**

Understanding the localization and engraftment of tumor cells at postintravasation stage of metastasis is of high importance in cancer diagnosis and treatment. Advanced fluorescent probes and facile methodologies for cell tracing play a key role in metastasis studies. In this work, we design and synthesize a dual-modality imaging dots with both optical and magnetic contrast through integration of a magnetic resonance imaging reagent, gadolinium(III), into a novel long-term cell tracing probe with aggregation-induced emission (AIE) in far-red/near-infrared region. The obtained fluorescent-magnetic AIE dots have both high fluorescence quantum yield (25%) and T_1 relaxivity (7.91 mM^{-1} s^{-1}) in aqueous suspension. After further conjugation with a cell membrane penetrating peptide, the dual-modality dots can be efficiently internalized into living cells. The gadolinium(III) allows accurate quantification of biodistribution of cancer cells via intraveneous injection, while the high fluorescence provides engraftment information of cells at single cellular level. The dual-modality AIE dots show obvious synergistic advantages over either single imaging modality and hold great promises in advanced biomedical studies.

1. Introduction

Although surgery and radiotherapy are able to control many malignant tumors at the primary sites, subsequent metastatic diseases always lead to poor prognosis as metastatic tumor cells can move from the primary neoplasm to a distant location in a living body.[1] In modern biomedical research, it has become a major concern to understand the cancer metastasis mechanism and process, which will dramatically benefit therapeutic treatments and improve patient outcomes.[2] Although mimic complete metastatic process can be achieved through xenograft studies with tumor cell lines known to metastasize in,vivo, such assays always suffer from poor quantification and slow completion.[3] As such, simple and direct experimental metastasis assays are ideal models to simulate the postintravasation stage of metastasis, in which tumor cells are injected into the bloodstream to monitor the location, distribution, and engraftment of administrated cells.[4] To understand the behavior of transplanted cells, different direct cell-labeling strategies involving optical, magnetic resonance (MR) and radionuclide imaging techniques have been reported.[5–7] However, each imaging approach has its own advantages and disadvantages. For instance, fluorescence imaging has high sensitivity but cannot provide quantitative evaluation of cell distribution upon transplantation, whereas MRI and radionuclide imaging provide desired tissue penetration depth but suffer from low sensitivity and resolution under single cellular level.[8] As compared with single-modal imaging probes, integration of two or more imaging modalities into a single probe will afford multimodal imaging probe with synergistic benefits, which is highly desirable in modern imaging.[9–11]

To date, fluorescent nanomaterials have been actively used as a platform to design multimodal imaging probes. Although inorganic quantum dots (QDs) have shown promising merits in fluorescence imaging (e.g., high fluorescence efficiency and remarkable resistance to photobleaching), the potential toxicity and fluorescence quenching phenomenon at low pH greatly impede their in vivo applications in real-world.[12,13] In previous studies, we have demonstrated that a novel class of photostable and biocompatible organic dots with aggregation-induced emission (AIE) in far-red/near-infrared (FR/NIR) region can greatly outperform its commercial inorganic QD counterpart in both in vitro and in vivo long-term cell tracing.[14] The AIE fluorogen is nonemissive in solution but becomes highly fluorescent in aggregates due to the restriction of intramolecular rotations

Dr. K. Li, Prof. B. Z. Tang, Prof. B. Liu
Institute of Materials Research and Engineering
3 Research Link, 117602, Singapore
E-mail: cheliub@nus.edu.sg
Dr. D. Ding, Prof. B. Liu
Department of Chemical and Biomolecular Engineering
National University of Singapore
117576, Singapore
C. Prashant, Dr. C.-T. Yang
Laboratory of Molecular Imaging
Singapore Bioimaging Consortium
11 Biopolis Way, #02-02 Helios, 138667, Singapore
W. Qin, Prof. B. Z. Tang
Department of Chemistry
Division of Biomedical Engineering
The Hong Kong University of Science & Technology
Clear Water Bay, Kowloon, Hong Kong, China
Prof. B. Z. Tang
SCUT-HKUST Joint Research Laboratory
Guangdong Innovative Research Team
State Key Laboratory of Luminescent Materials and Devices
South China University of Technology
Guangzhou 510640, China

DOI: 10.1002/adhm.201300135

that opens the radiative decay channel.[15] The AIE phenomenon is opposite to the notorious aggregation-caused quenching effect of organic fluorophores,[16,17] making AIE fluorogens ideal materials for highly fluorescent nanoparticles. In addition, the versatile encapsulation matrices with different surface functional groups, e.g., –maleimide (–Mal), $–NH_2$, and –COOH terminated distearoyl-*sn*-glycero-3-phosphoethanolamine-poly(ethylene glycol) (DSPE-PEG) derivatives, facilitate further functionalization to achieve the goal of multimodal imaging. As DSPE-PEG derivatives with different terminal groups have been reported to form heterogeneous patches on nanoparticle and microparticle surfaces,[18] this property is beneficial to sequential surface functionalization with minimal steric interference.

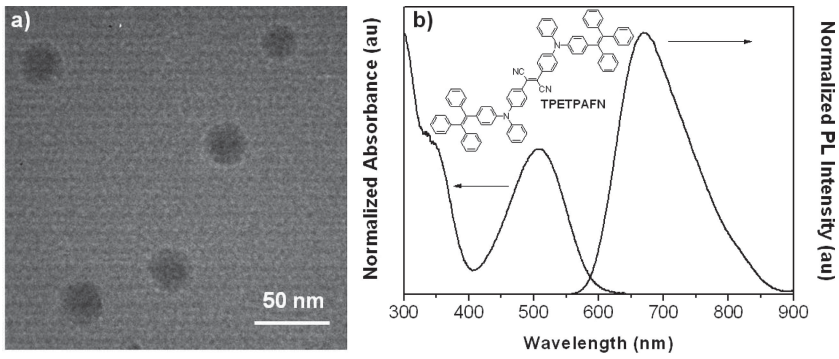

Figure 1. a) HR-TEM image of AIE dots in water. b) UV--vis absorption and PL spectra of AIE dots in water (λ_{ex} = 510 nm). The inset shows the chemical structure of TPETPAFN.

In this contribution, we fabricated fluorescent-magnetic dual-modality AIE dots for in vivo tumor cell metastasis studies. A mixture of amine- and Mal-terminated DSPE-PEG (DSPE-PEG-NH_2 and DSPE-PEG-Mal) was used as the encapsulation matrix to synthesize biocompatible AIE dots with different surface functionalities. Diethylenetriaminepentaacetic (DTPA) dianhydride was employed to conjugate with amine groups on AIE dot surface for further chelation of gadolinium(III) to endow magnetic contrast, whereas the maleimide groups were used to immobilize the cell penetrating peptide via maleimide-thiol coupling reaction to enhance the living cell labeling efficiency. The obtained Tat-Gd-AIE dots were further used to label C6 glioma cells before being injected into mice through tail vein to evaluate the cell distribution and engraftment at the postintravasation stage of metastasis. Ex vivo analysis reveals that the incorporation of Gd(III) allows accurate quantification of transplanted cell biodistribution and the high fluorescence of AIE dots ensures excellent single cell imaging to provide valuable information of cancer cell engraftment in organ tissues. The developed dual-modality AIE dots not only provide mutual advantages in metastasis analysis but also inspire further exploration of multimodal imaging dots for in vivo monitoring of transplanted cells with both high temporal and spatial resolution.

2. Results and Discussion

2.1. Synthesis and Characterization of Dual-Modality AIE Dots

The AIE fluorogen, TPETPAFN, was synthesized according to literature.[14] The AIE dots were synthesized through a nanoprecipitation approach reported by our group.[19] 1,2-Distearoyl-*sn*-glycero-3-phosphoethanolamine-*N*-[amino(polyethylene glycol)-2000] (DSPE-PEG_{2000}-NH_2) and 1,2-distearoyl-*sn*-glycero-3-phosphoethanolamine-*N*-[maleimide(polyethylene glycol)-2000] (DSPE-PEG_{2000}-Mal) were used to encapsulate TPETPAFN molecules to afford AIE dots with surface amine and maleimide groups for further conjugation. In brief, TPETPAFN, DSPE-PEG_{2000}-NH_2, and DSPE-PEG_{2000}-Mal (1 mg each) were dissolved in tetrahydrofuran (THF) solution. The THF solution was rapidly mixed with water, followed by sonication to yield AIE dots with abundant surface amine and maleimide groups. After THF evaporation, the dots were filtered through a 0.2 μm syringe filter. High-resolution transmission electron microscopy (HR-TEM) image reveals that the AIE dots are in spherical shape (**Figure 1**), with an average particle size of 31.7 ± 2.1 nm. The water suspension of AIE dots shows maximum absorption and emission at 512 and 670 nm, respectively, with an intense emission tail till 900 nm. The quantum yield of AIE dots in water was measured to be 25% using 4-(dicyanomethylene)-2-methyl-6-(p-dimethylaminostyryl)-4H-pyran in methanol as a standard (Φ_F = 43%).[20]

To integrate the MR contrast with the fluorescent AIE dots, DTPA dianhydride was used to conjugate with surface amine groups for chelation of Gd(III). The obtained Gd(III)-chelated dots were then modified with HIV-1 Tat peptide (RKKRRQRRRC) through conjugation between maleimide groups on dot surface and thiol groups at C-terminus of Tat peptide. The Gd(III) content in the finally obtained Tat-Gd-AIE dots was quantified using ion coupled plasma-mass spectrometry (ICP-MS). The results reveal that the number of successfully chelated Gd(III) ions on each dot is estimated to be ≈136. To investigate the stability of chelate Gd(III) on Tat-Gd-AIE dots, 1 mL of the Tat-Gd-AIE dot suspension was dialyzed against water for 48 h at 37 °C. ICP-MS results suggest that the Gd(III) concentration in the dot suspension keeps consistent before and after dialysis, indicating that the chelate Gd(III) elements are stable on Tat-Gd-AIE dot surface. High-performance liquid chromatography (HPLC) was employed to determine the number of Tat peptide conjugated on the dot surface, suggesting that there are ≈850 peptide molecules on each dot.

2.2. Cell Imaging and Cytotoxicity

The performance of Tat-Gd-AIE dots for direct cell labeling was first examined using C6 glioma cells and the fluorescence images were acquired by confocal as shown in **Figure 2**. Upon 12 h incubation with 2×10^{-9} M Tat-Gd-AIE dots at 37 °C, intense fluorescence signal can be detected from C6 glioma cells upon excitation at 514 nm (1 mW). The 3D confocal image of Tat-Gd-AIE dot-labeled C6 cells was also obtained, indicating that the dots were internalized into the cells to emit intense fluorescence signal (Figure S1, Supporting Information). It is noteworthy that no

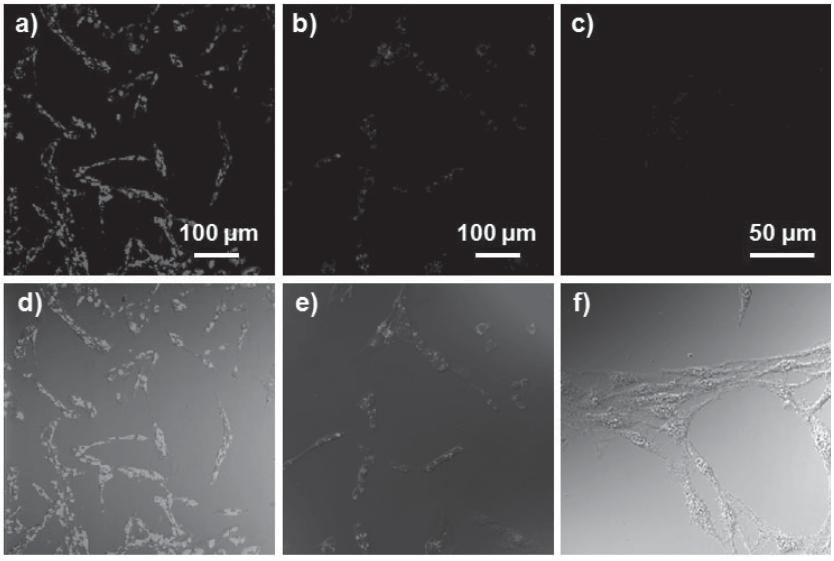

Figure 2. Confocal images of C6 glioma cells after incubation with 2×10^{-9} M a) Tat-Gd-AIE dots and b) Gd-AIE dots for 12 h at 37 °C, respectively. c) Cells without incubation with Tat-Gd-AIE dots. d–f) The overlay for a–c) with their respective transmittance images, respectively.

autofluorescence can be detected from the cells without incubation with Tat-Gd-AIE dots (Figure 2c), which further proves that the intense fluorescence in Figure 2a is from the dots internalized into C6 cells. Gd-AIE dots without Tat peptide functionalization were also used as a control group to highlight the direct cell labeling ability of Tat-Gd-AIE dots. As shown in Figure 2b, under the same experimental conditions, only very weak fluorescence signal can be detected from the Gd-AIE dot-treated cells, indicating that at the same dot concentration, much fewer Gd-AIE dots were internalized into C6 cells as compared with that for Tat-Gd-AIE dots. As a result, the surface conjugation of Tat peptide on fluorescent dots plays a crucial role in enhancing living cell internalization efficiency, which is desirable for cell tracing.

A major concern in fluorescence imaging of biotargets is the biocompatibility of the probes. To obtain reliable experimental results, fluorescent probes should possess very low toxicity to target cells during cell tracing studies. To evaluate the cytotoxicity of pure AIE dots without surface modification and Tat-Gd-AIE dots, methylthiazolyldiphenyltetrazolium bromide (MTT) assays were employed to determine the metabolic viability of C6 glioma cells after incubation with 1, 2, and 4×10^{-9} M dots for 24 and 48 h. As shown in Figure S2 (Supporting Information), the cell viability remains above 90% after 48 h incubation with the dual-modality dots, indicating their low cytotoxicity under the studied conditions.

2.3. Cell Tracing in Mice

The performance of Tat-Gd-AIE dots in in vivo cell tracing was then evaluated using an animal model. After incubation with 2×10^{-9} M Tat-Gd-AIE dots in culture medium at 37 °C for 12 h, living C6 glioma cells were trypsinalized and suspended in freshly prepared culture medium, followed by immediate intravenous injection into the mice through tail vain (1.5×10^6 cells in 0.2 mL of medium for one mouse). After designated time intervals, the mice (Four groups, $n = 3$ for each group) were sacrificed and various organs including heart, liver, spleen, lung, and kidney were isolated and imaged using an IVIS Spectrum Imaging System (**Figure 3**a). At each time point post injection, intense fluorescence is observed from the lung and liver while the spleen also emits visible fluorescence signal upon excitation at 560 nm, indicating the preferential accumulation of injected cells in these organs. On the contrary, fluorescence signal from the kidney and heart is negligible at all time points. It is noteworthy that the obvious accumulation of injected cells in the lung is consistent with the results from previously reported cell transplantation studies, suggesting that intravenously delivered cells are likely to be trapped inside the pulmonary system due to the pulmonary microvascular barrier.[21,22]

To further study the biodistribution of transplanted cells in living animal bodies, the collected organs were decomposed by concentrated nitric acid and analyzed using ICP-MS to measure the Gd(III) contents. The percentage of cells engrafted in each organ from the total amount of cells localized in all the five organs was first calculated, suggesting that ≈35% and 48% of the cells are engrafted in the lung and liver at 1 h post injection, respectively. On the other hand, only ≈17% of the cells are in heart, spleen, and kidney. The Gd(III) concentrations in organs at all the time points were further studied to investigate the time course of accumulation of the C6 cells. As shown in Figure 3b, the concentrations of Gd(III) in lung, spleen and

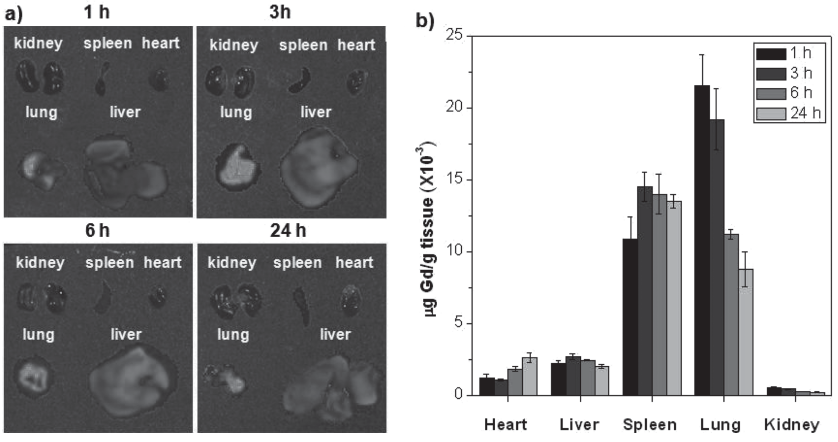

Figure 3. a) Representative ex vivo fluorescence images of various organs collected from the mice injected with Tat-Gd-AIE dots-labeled C6 glioma cells at 1, 3, 6, and 24 h post injection. b) The concentrations of Gd(III) in heart, liver, spleen, lung, and kidney at 1, 3, 6, and 24 h post injection, respectively.

liver tissues are determined to be 21.5, 10.9, and 2.2×10^{-3} μg g^{-1} tissue at 1 h post injection of the cells, respectively. It should be noted that the concentration of Gd(III) in each organ is normalized to per gram tissue and the concentration of Gd(III) in liver is much lower than that in spleen (the ratio of $Mass_{liver}$ to $Mass_{spleen}$ is ≈100:1). Moreover, the concentration of cells accumulated in lung decreased at 6 h post injection, whereas that in other organs are relatively consistent as time elapses. This agrees with the previous reports that injected cells were first captured by lung or liver and then released from the organs to enter circulation for further migration.[23,24] As compared with semiquantitative evaluation using fluorescence techniques, the incorporation of Gd(III) in AIE dots allows accurate quantitation of the biodistribution of transplanted cells.

2.4. Localization of Cells in Organ Tissues

To investigate the localization of injected cells in organs, one mouse was sacrificed at 24 h post injection and the lung, spleen, liver, heart, and kidney tissues were collected for study using confocal laser scanning microscopy. As shown in Figure S3 (Supporting Information), intense red fluorescent spots are clearly observed in the collected organ tissues, indicating the engraftment of injected cells in the animal body. In the enlarged confocal image of lung tissue (Figure S3f, Supporting Information), three individual cells labeled by Tat-Gd-AIE dots in the view can be seen to engraft in the tissue while the surrounding tissue cells are not fluorescent. These results clearly demonstrate the ability of Tat-Gd-AIE dots to monitor cell engraftment after transplantation with high resolution and sensitivity under single cellular level, which is of high importance in cancer metastasis and cell therapy studies.

Furthermore, the deep tissue imaging was also performed upon exciting the lung at 560 nm using one-photon excited fluorescence microscope. To study the efficient penetration depth of Tat-Gd-AIE dots in deep tissue, fluorescence signal from the lung was collected layer-by-layer at 3 μm interval. As shown in Figure S3g (Supporting Information), the 3D color-coded projection of deep tissue image indicates that the fluorescence of labeled cells can be detected up to 150 μm depth. The eminent performance of Tat-Gd-AIE dots in one-photon excited deep tissue imaging can be attributed to the high molar extinction coefficient at long wavelength (3.5×10^7 M^{-1} cm^{-1} at 560 nm).

2.5. Magnetic Resonance Imaging

The magnetic property of Tat-Gd-AIE dots was investigated by measuring longitudinal relaxation time (T_1) of water protons as a function of Gd(III) concentration in aqueous solutions using a 7-Tesla Bruker ClinScan MR scanner. **Figure 4**a shows the T_1-weighted MR images of Tat-Gd-AIE dots in water suspensions at various Gd(III) concentrations, indicating that the signal intensity gradually increases upon increasing the Tat-Gd-AIE dot concentration. The T_1 relaxivity (r_1) value that refers to the amount in $1/T_1$ per Gd(III) unit concentration of agent is calculated to be 7.91 mM^{-1} s^{-1} (Figure 4b). The spin–spin relaxation time (T_2) of the dual-modality dots was also calculated, giving

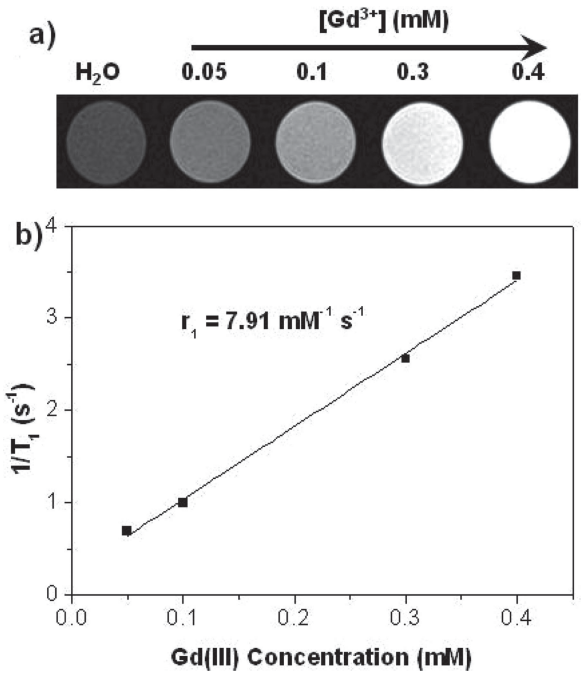

Figure 4. a) T_1-weighted MR images of Tat-Gd-AIE dots at various Gd(III) concentrations of 0, 0.05, 0.1, 0.3, and 0.4×10^{-3} M. b) Plot of water proton longitudinal relaxation rate ($1/T_1$) of Tat-Gd-AIE dots as a function of Gd(III) concentration.

a T_2 relaxivity (r_2) value of 10.9 mM^{-1} s^{-1}. As a result, the r_2/r_1 value is below 2, indicating that the probe belongs to positive contrast reagent.[25] Under the same experimental conditions, Dotarem®, a commercial Gd(III)-complex of T_1 contrast reagent, shows a r_1 value of 3.761 mM^{-1} s^{-1}. Overall, the small r_2/r_1 value of Tat-Gd-AIE dots and higher r_1 value as compared with Dotarem® endow the dual-modality probes great potential to serve as a novel T_1 contrast reagent in bioimaging tasks.

In vivo MRI experiments were further conducted on an animal model and the C6 cells labeled by Tat-Gd-AIE dots (3×10^6 cells) were injected into the mice following the same experimental protocol as described in the fluorescence imaging. The cross-sectional T_1-weighted MR images of mice were recorded at 7.0 T before and after injection of Tat-Gd-AIE dot-labeled cells. As shown in Figure S4 (Supporting Information), the liver is not lightened at 1 and 24 h post injection and the brightness of these organs remains similar to that of the muscle tissues. The negative MRI results could be attributed to the fact that the Gd(III) content injected into the mice is lower than the detection threshold[26] (ICP-MS result suggests that there are ≈1.2×10^{-4} μmol Gd(III) in total 3×10^6 cells injected into one mouse). These results clearly indicate that MRI suffers from low sensitivity in direct cell tracing.[27] However, the incorporation of Gd(III) can provide precise information of the biodistribution of transplanted cells.

3. Conclusions

In this work, we report a general strategy to synthesize dual-modality dots through attaching DTPA-Gd(III) ligands to the

surface of fluorescent AIE dots and demonstrate their great potential in cell tracing studies using an animal model to mimic postintravasation stage of metastasis. Upon surface conjugation with Tat peptides, the obtained Tat-Gd-AIE dots have shown greatly enhanced living cell internalization efficiency. The incorporation of Gd(III) on dual-modality imaging dots allows accurate quantification of the biodistribution of injected cancer cells. On the other hand, the high brightness of the dots facilitates ex vivo imaging of transplanted cells at single cell level, which is of high importance to obtain information of the engrafted metastatic cancer cells in the organs. Although the Tat-Gd-AIE dots have been proven to be an efficient T_1 contrast reagent with desired longitudinal relaxation time, the labeled cells can not be detected through MRI upon intravenous injection into the mice, due to the relatively low sensitivity of MRI and the insufficient amount of Gd(III) in the injected cells. To enhance the capability for Gd(III) chelation to realize in vivo cell tracing through MRI, optimization of the AIE dot formulation (e.g., attachment of hyperbranched polyglycerols to AIE dot surface to afford more active sites for conjugation with DTPA-Gd) will be highly desired. Taking advantage of the versatile surface functionalities of AIE dots, integration of highly sensitive imaging modalities (e.g., radioactive reagent) into the AIE dots is also expected to provide both high spatial and temporal resolution to benefit in vivo cell tracing.

4. Experimental Section

Materials: DSPE-PEG_{2000}-$NH_2$and DSPE-PEG_{2000}-Mal were purchased from Avanti Polar Lipids, Inc. THF, dimethyl sulfoxide (DMSO), Dulbecco's modified eagle medium (DMEM), gadolinium(III) chloride hexahydrate, DTPA dianhydride, diphenylamine, 3-(4,5-dimethylthiazol-2-yl)-2,5-diphenyl tetrazolium bromide (MTT), penicillin-streptomycin solution, fetal bovine serum, and trypsin-EDTA solution were purchased from Sigma–Aldrich. A cell penetrating peptide, HIV-1 Tat (49–57) with C-terminus modified with cysteine (RKKRRQRRRC), was a commercial product customized by GenicBio, China. Milli-Q water was supplied by Milli-Q Plus System (Millipore Corporation, Bredford, MA). Rat C6 glioma cells were provided by American Type Culture Collection. Male SCID mice were obtained from the Biological Resource Centre (Biopolis, Singapore). Mice were housed in groups (5 per cage) and provided with standard mouse chow and water at libitum. The cages were maintained in a room with controlled temperature (25 ± 1 °C) and a 12 h light/dark cycle (light on at 7:00 am). All animal experiments were performed in compliance with guidelines set by the Institutional Animal Care and Use Committee (IACUC), SingHealth.

Characterization: The UV–vis spectra were recorded on a Shimadzu UV-1700 spectrometer. The fluorescence spectra were measured using a fluorometer (LS-55, PerkinElmer, USA). Fluorescence quantum yield of the AIE dots was determined using 4-(dicyanomethylene)-2-methyl-6-(*p*-dimethylaminostyryl)-4H-pyran in methanol (43%) as a standard. Average particle sizes were determined by laser light scattering with a particle size analyzer (90 Plus, Brookhaven Instruments Co., USA) at a fixed angle of 90° at room temperature. HR-TEM images were recorded using a JEM-2010F microscopy (JEOL, Japan) with an accelerating voltage of 200 kV.

Synthesis of Surface-Functionalized AIE Dots: TPETPAFN, DSPE-PEG_{2000}, and DSPE-PEG_{2000}-NH_2 (1 mg for each) were dissolved in 1 mL of THF to form homogeneous solution. The solution was added into 9 mL of water and the mixture was sonicated using a microtip probe sonicator (XL2000, Misonix Incorporated, NY) for 60 s at 12 W output. The obtained dot suspension was vigorously stirred at room temperature overnight in fumehood at 800 rpm to evaporate the organic solvent to yield TPETPAFN dots (AIE dots) with surface amine and maleimide groups in 8 mL of water. The AIE dots were filtered using a 0.2 μm syringe driven filter to purify. 1 mL of borate buffer (pH = 8.5) and 200 μL of DTPA dianhydride (2 mg) solution in DMSO was added into 4 mL of AIE dots water suspension and the mixture was stirred at room temperature for 24 h, followed by dialysis against MilliQ water using a 3.5 kDa molecular weight cutoff dialysis membrane for 2 d. Gadolinium(III) chloride hexahydrate (4 mg) was further added to the DTPA-AIE dots suspension for 24 h at room temperature. The free Gd(III) was removed by dialysis against MilliQ water for 2 d using a 3.5 kDa molecular weight cutoff dialysis membrane. To attach HIV-1 Tat peptides on the dots, Gd-AIE dots were mixed with HIV1-Tat peptide (0.1 μmol) and stirred overnight. After dialysis using a 3.5 kDa molecular weight cutoff dialysis membrane, the final product, Tat-Gd-AIE dots were obtained and concentrated through freeze-drying. The water after each run of dialysis was collected and concentrated for HPLC measurements to determine the number of peptides conjugated on dot surface. The Gd(III) content in Tat-Gd-AIE dots was determined by ICP-MS.

In Vitro Cell Imaging: C6 glioma cells were precultured in four-well confocal chamber (Costar, IL, USA) to achieve 80% confluence. The medium was then removed and the cells were washed twice with 1× PBS buffer, followed by addition of 2×10^{-9} M Tat-Gd-AIE dots in DMEM for incubation at 37 °C. After 12 h, the cell monolayer was washed with 1× PBS buffer and fixed by 75% ethanol for 20 minutes. The confocal images were obtained using Leica TCS SP 5X upon excitation at 514 nm (1 mW) and the fluorescence signal was collected using a 550–800 nm bandpass filter.

Cytotoxicity Studies: Cytotoxicity of Tat-Gd-AIE dots was evaluated using C6 glioma cells through MTT assay. In brief, C6 glioma cells were seeded in 96-well plates (Costar, IL, USA) at a density of 4×10^4 cells mL^{-1}. After 24 h incubation, the medium was discarded and Tat-Gd-AIE dots in DMEM with various concentrations were added into each sample wells for further incubation at 37 °C. To eliminate the UV absorption interference of TPETPAFN at 570 nm, the cells incubated with a series of Tat-Gd-AIE dots at the same doses but not post treated by MTT were used as the control. After the designated time intervals, the sample wells were washed twice with 1× PBS buffer and 100 μL of freshly prepared MTT (0.5 mg mL^{-1}) solution in culture medium was added into each well. After 3 h incubation in the incubator, the MTT medium solution was carefully removed, followed by addition of 100 μL of DMSO into each well and the plate was gently shaken for 10 min at room temperature to dissolve all the precipitates formed. The absorbance of MTT at 570 nm was monitored by the microplate reader (Genios Tecan). Cell viability was expressed by the ratio of the absorbance of the cells incubated with Tat-AIE dot suspension to that of the cells incubated with culture medium only.

In Vivo Cell Tracing: All animal experiments were performed in compliance with guidlines set by the Institutional Animal Care and Use Committee (IACUC), Sigapore General Hospital. C6 glioma cells were cultured in 6-well plates (Costar, IL, USA) to achieve 80% confluence. After medium removal and washing with 1× PBS buffer, 2×10^{-9} M Tat-Gd-AIE dots in DMEM medium were then added to the wells for incubation at 37 °C. After 12 h, the cells were washed twice with 1× PBS buffer and detached by 1× trypsin. Trypsin was discarded through centrifugation at 2000 rpm for 5 min and the labeled cells were resuspended in culture medium. The labeled C6 glioma cells (0.1 mL, 1×10^6 cells) were then intravenously injected into each mouse. Three mice were used for each group. After designated time intervals post injection, the mice were imaged using an IVISSpectrum imaging system (Caliper Life Sciences) while under anesthesia. The fluorescence images were recorded with 1 s exposure using a filter 660/20 nm upon excitation at 535 nm. Scans were carried out on 1, 3, 6, and 24 h, respectively. The autofluorescence was removed using the software of IVIS Spectrum imaging system.

Ex Vivo One-Photon Excited Fluorescence Imaging: After in vivo imaging at designated time intervals upon injection of labeled C6 glioma cells, the mice were euthanized with CO_2 to harvest the organs (heart, kidney, spleen, lung, and liver) for isolated tissue imaging using the IVIS®

Spectrum imaging system. The organs collected at 24 h post injection of labeled C6 glioma cells were then fixed in 4% paraformaldehyde and imaged using confocal microscope (Leica TCS SP 5X) upon excitation at 560 nm with a 600–800 nm bandpass filter. The one-photon excited fluorescence images of consecutive layers with approximately 3 μm interval were recorded to generate 3D colored projection to demonstrate the penetration depth of fluorescence signal from Tat-Gd-AIE dots-labeled cells in the lung.

In Vitro MRI Studies: In vitro MRI studies were conducted on a 7Tesla MRI Bruker ClinScan using a 72 mm volume coil. The longitudinal relaxation time (T_1) of the Gd-NPs in aqueous solutions with different concentrations of Gd(III) (0.0165–0.5 $\times 10^{-3}$ M) were measured using an inversion recovery spin echo sequence with TR = 5000 ms, TE = 7 ms, and inversion times of 31, 150, 300, 700, 1200, 1800, 2400, 3000, 3600, 4000, 4500, and 4900 ms. The transverse relaxation time (T_2) was determined using a multiple spin echo sequence with TR = 5000 ms, TE = 12.9 ms, and NE = 14. The T_1 and T_2 relaxivity values (r_1 and r_2) were obtained from linear least-squares determination of the slope of $1/T_1$ relaxation time (s^{-1}) and $1/T_2$ relaxation time (s^{-1}) versus the Gd(III) concentration ($\times 10^{-3}$ M) plot, respectively.

In Vivo MRI Studies: The labeled Tat-Gd-AIE dot-labeled C6 glioma cells (0.2 mL, 3×10^6 cells) were intravenously injected into the mice. After designated time intervals post injection, the MR images of mice under anesthesia were conducted on a 7Tesla MRI Bruker ClinScan. T_1-weighted images were acquired at 1 and 24 h.

Supporting Information

Supporting Information is available from the Wiley Online Library or from the author.

Acknowledgements

The authors are grateful to the support from the Institute of Materials Research and Engineering of Singapore (IMRE/12-8P1103, IMRE/13-8P1104), the Singapore National Research Foundation (R-279-000-390-281), the Research Grants Council of Hong Kong (603509, HKUST2/CRF/10, 604711 and N_HKUST620/11), the National Science Foundation of China (20974028) and the Guangdong Innovative Research Team Program (201101C0105067115). The authors thank Tong Yan from the confocal microscopy lab at the Centre for BioImaging Sciences (CBIS) in NUS for technical support in confocal imaging experiments.

Received: April 12, 2013
Published online: July 9, 2013

[1] S. Paget, *Lancet* **1889**, *1*, 571.
[2] A. F. Chambers, A. C. Groom, I. C. MacDonald, *Nat. Rev. Cancer* **2002**, *2*, 563.
[3] D. Welch, *Clin. Exp. Metastasis* **1997**, *15*, 272.
[4] P. S. Steeg, *Nat. Med.* **2006**, *12*, 895.
[5] J. V. Terrovitis, R. R. Smith, E. Marban, *Circ. Res.* **2010**, *106*, 479.
[6] C.-Y. Fang, V. Vaijayanthimala, C.-A. Cheng, S.-H. Yeh, C.-F. Chang, C.-L. Li, H.-C. Chang, *Small* **2011**, *7*, 3363.
[7] C. Villa, S. Erratico, P. Razini, A. Farini, M. Meregalli, M. Belicchi, Y. Torrente, *Tissue Eng. Part B* **2011**, *17*, 1.
[8] A. Bhirde, J. Xie, M. Swierczewska, X. Chen, *Nanoscale* **2011**, *3*, 142.
[9] J.-S. Choi, J. C. Park, H. Nah, S. Woo, J. Oh, K. M. Kim, G. J. Cheon, Y. Chang, J. Yoo, J. Cheon, *Angew. Chem., Int. Ed.* **2008**, *47*, 6259.
[10] K. Li, D. Ding, D. Huo, K. Y. Pu, N. N. P. Thao, Y. Hu, Z. Li, B. Liu, *Adv. Funct. Mater.* **2012**, *22*, 3107.
[11] H.-Y. Lee, Z. Li, K. Chen, A. R. Hsu, C. Xu, J. Xie, S. Sun, X. Chen, *J. Nucl. Med.* **2008**, *49*, 1371.
[12] N. Lewinski, V. Colvin, R. Drezek, *Small* **2008**, *4*, 26.
[13] Y. S. Liu, Y. H. Sun, P. T. Vernier, C. H. Liang, S. Y. C. Chong, M. A. Gundersen, *J. Phys. Chem. C* **2007**, *111*, 2872.
[14] K. Li, W. Qin, D. Ding, J. Geng, J. Liu, X. Zhang, H. Liu, B. Liu, B. Z. Tang, *Sci. Rep.* **2013**. *3*, 1150.
[15] Y. Hong, J. W. Y. Lam, B. Z. Tang, *Chem. Commun.* **2009**, 4332.
[16] Y. Hong, J. W. Y. Lam, B. Z. Tang, *Chem. Soc. Rev.* **2011**, *40*, 5361.
[17] W. Qin, D. Ding, J. Liu, W. Z. Yuan, Y. Hu, B. Liu, B. Z. Tang, *Adv. Funct. Mater.* **2012**, *22*, 771.
[18] C. Salvador-Morales, P. M. Valencia, W. Gao, R. Karnik, O. C. Farokhzad, *Small* **2013**, *25*, 511.
[19] K. Li, Y. Jiang, D. Ding, X. Zhang, Y. Liu, J. Hua, S.-S. Feng, B. Liu, *Chem. Commun.* **2011**, *47*, 7323.
[20] J. M. Drake, M. L. Lesiecki, D. M. Camaioni, *Chem. Phys. Lett.* **1985**, *113*, 530.
[21] U. M. Fischer, M. T. Harting, F. Jimenes, W. O. Monzon-Posadas, H. Xue, S. I. Savitz, G. A. Laine, C. S. Cox, Jr., *Stem Cells Dev.* **2009**, *18*, 683.
[22] E. B. Voura, J. K. Jaiswal, H. Mattoussi, S. M. Simon, *Nat. Med.* **2004**, *10*, 993.
[23] L. Weiss, *Int. J. Cancer* **1980**, *25*, 385.
[24] L. Weiss, P. M. Ward, J. C. Holmes, *Int. J. Cancer* **1983**, *32*, 79.
[25] A. Favier, F. D'Agosto, M.-T. Charreyre, C. Pichot, *Polymer* **2004**, *45*, 7821.
[26] L. Faucher, M. Tremblay, J. Lagueux, Y. Gossuin, M.-A. Fortin, *ACS Appl. Mater. Interfaces* **2012**, *4*, 4506.
[27] M. F. Kircher, S. S. Gambhir, J. Grimm, *Nat. Rev. Clin. Oncol.* **2011**, *8*, 677.

